Jurnal Teknologi

Full paper

Computational Fluid Dynamics (CFD) Mesh Independency Technique for a Propeller Characteristics in Open Water Condition

M. Nakisa[a,c], A. Maimun[b*], Yasser M. Ahmed[a,d], F. Behrouzi[a], Jaswar[a], A. Priyanto[a]

[a]Faculty of Mechanical Engineering, UniversitiTeknologi Malaysia, 81310 UTM Johor Bahru, Johor, Malaysia
[b]Marine Technology Center, UniversitiTeknologi Malaysia, 81310 UTM Johor Bahru, Johor, Malaysia
[c]Faculty of Engineering, Islamic Azad University, Boushehr Branch, Boushehr, Iran
[d]Faculty of Engineering, Alexandria University, Alexandria, Egypt

*Corresponding author: adi@fkm.utm.my

Article history

Received :25 December 2014
Received in revised form :
25 March 2015
Accepted :15 May 2015

Graphical abstract

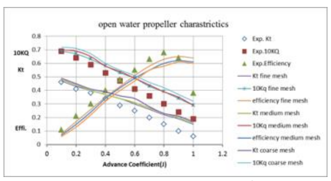

Hydrodynamic propeller performance
In open water

Abstract

This paper numerically investigated mesh refinement method in order to obtain a mesh independent solution for a marine propeller working in open water condition.Marine propeller blade geometries, especially of LNG carriers, are very complicated and determining the hydrodynamic performance of these propellers using experimental work is very expensive, time consuming and has many difficulties in calibration of marine laboratory facilities. The present research workhas focused on the hydrodynamic propeller coefficients of a LNG carrier Tanaga class such as K_t, K_q and η, with respect to the different advance coefficient (j). Finally, the results of numerical simulation in different mesh density that have been calculated based on RANS (Reynolds Averaged Navier Stocks) equations, were compared with existing experimental results, followed by analysis and discussion sections. As a result the maximum hydrodynamic propeller efficiency occurred when j=0.84.

Keywords: Numerical simulation; mesh independency; propeller performance; RANS equation

1.0 INTRODUCTION

Over the past ten years or so there has been an increasingly more rapid advances in the applications of the computational fluid dnamics for investigating the rotational objects such as turbines and propeller characteristics of ships.The computational fluid dynamics is based on the concept of Reynolds averaging of the unsteady Navier-Stockes equations, widely known as (URANS) wich are considered by Leishman[1,2] to be the most appropriate method for analyzing nonlinear viscous flows providing that a suitable turbulence model is employed.

Reynolds Averaged Navier-Stokes (RANS) method coupled with turbulence model has been widely used in the past. A number of numerical studies relating to propeller characteristics issues have been carried out based on RANS equations with early example found in Kerwin[3] and Kim [4]. Since then, numerical error and resolution of flow details have been significantly improved. Taking advantage of modern computer, CFD software is now available commercially with the solution turnaround time dramatically reduced.

Viscid and in-viscid flows with CFD (Computational Fluid Dynamics) are widely used for design aims and the experimental tests to be conducted for the last step of research work. Considering to in maritime applications, numerical methods can be performed to estimate the flow pattern around ship hulls, rudders, propellers and appendages.

The other ways to predict the ship resistance in open water and ice condition is using upper and lower fore bulbous angles, entrance angle and spreading angles in analytical method with propeller and without. Also Jaswar (2014) emphesized on analaytical investigation of deepwater subsea pipelines affected by water speed crossing in seabed[3,4].

Abyn *et al*., (2014) studied on effect of mesh number on accuracy of semi submersible motion to find the fine mesh density for approach the accure results[5].In case of the visualisation of flow pattern around merchant ship's propellers, computational fluid dynamics based on Lifting-Surface theory for first step is commonly used[6-8]. The viscid RANS (Reynolds Average Navier Stocks) equation solution used later comes to function after (Kerwin *et al.* 1978).

Reynolds Average Navier Stocks is introduced for the application of numerical technics in fluid mechanics and improvement for computer performances[9-13].

Modelling, geometry, computational domains, boundary conditions, topology, meshing method and mesh size and turbulent method have significant effects on a fruitful numerical analysis and accuracy of simulation. Meshing strategy is divided in two divisions. Hybrid unstructured a mesh means that the tetrahedral elements for flow fluid fields, while structured mesh means that the hexahedral mesh is totally used for meshing on the solid surfaces. In contrast, the results of simulations with structured mesh elements usually have more accuracy than tetrahedral mesh elements results.

Unstructured mesh elements production is almost automatic while hexahedral mesh elements generation is not automatic and should be generated manually. On the other hand, for flow field meshing, sometimes, the geometry is not compatible to use the hexahedral mesh elements, so unstructured mesh elements have better results and convergence of solution is nice. Therefore, we used the hybrid unstructured mesh elements for rotational domain, in which we utilized the stationary and rotational domain for full scale propeller simulation for propeller with five blades.

CFD simulation data were verified with existing test results. This study focuses on hydrodynamic propeller performance and characteristics in open water condition. The hydrodynamic values such as thrust (Kt) and torque (Kq) coefficients and the other selected values were measured in this numerical research work.

2.0 PROPELLER MODEL

The propeller model with full scale principles was simulated in this numerical work using finite volume method. The diameter (D) of considered propeller was 7.7 m and the diameter of hub (Dhub) was 0.17D, plus the rotation of the propeller was made right handed to make the thrust. Pitch ratio design (P/D) was 0.94 and blade ration (EAR) was 0.88.

The propeller drawing is depicted in Figure 1 and the Table 1 shows the geometric characteristics.

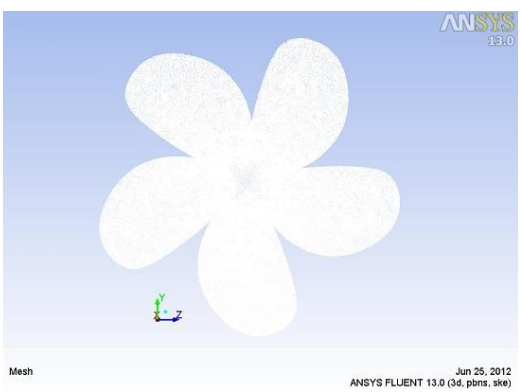

Figure 1 Front view of propeller

The centreline of the propeller was allocated on the centre point and reference of the Cartesian coordinate. The x-direction was associated with centreline of the propeller, y-direction was arranged with upward of the propeller and z-direction followed the right handed Cartesian coordinate system that showed to port side, as shown in Figure 1.

Table 1 Propeller geometric parameters

Parameters	Dimension
Z	5
D	7.7 m
Dhob	1.28 m
Br	0.17
P/D	0.94
Ae/A0	0.88
R	15 Deg.

3.0 BOUNDARY CONDITION

ANSYS-Fluent 13 was applied to numerical prediction of the hydrodynamic propeller characteristics which solved the RANS equation by Finite Volume Method(FVM). Figure 2 and Table 2 show the scheme and dimensions of computational domain to simulate the propeller in open water, respectively.

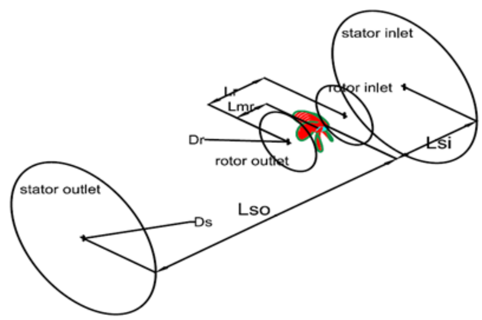

Figure 2 scheme of computational domain

Multiple Frame of Reference (MRF) was applied in the numerical estimation of the flow around the ship propeller technique. In accordance to uniform and homogeneous flow around the ship propeller, mathematical predictions didbased on focusing on total blades, similarly.

Table 2 Dimensions of computational domain

Value	Rotational	Stationary
Dr	1.44 D	
Lmr	1.5 D	
Lr	3 D	
Ds		10 D
Lsi		3 D
Lso		5 D
d		1.7 D

The stationary and rotating parts are called stationary and rotating, respectively.[10] Table 2 shows the characteristics of the domain of propeller: D is the propeller diameter and L_{mr} is the axial length of outlet in rotational domain, as shown in Figure 2. It was considerable to remove the wall effect on results. The dimensions of boundaries were considered far enough from the propeller in the stationary part. Figure 3 and Figure 4 show the rotational and stationary with propeller domainsin mesh condition.

Figure 3 Rotational and Stationary domain

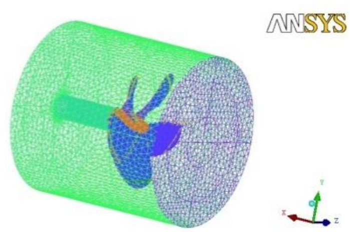

Figure 4 propeller in rotational domain mesh

Three mesh elemnts numbers are shown in Table 3 which three dimentional gridsare generated via unstructured tetrahedral mesh generation technique usingAnsys- ICEMCFD14.0**.**

Table 3 Mesh description

Status	No. of Mesh elements	No. of Nodes
Fine(1)	2,758,980	3,453,210
Medium(2)	1,791,132	1,979,025
Coarse(3)	920,854	984,349

4.0 NUMERICAL METHOD

In Cartesian tensor form the general RANS equation for continuity can be written as,

$$\frac{\partial \rho}{\partial t}+\frac{\partial(\partial u_i)}{\partial x_i}=0 \qquad (1)$$

and equation for momentum become:

$$\frac{\partial(\rho u_i)}{\partial t}+\frac{\partial(\rho u_j u_i)}{\partial x_j}= -\frac{\partial \rho}{\partial x_i}+\frac{\partial}{\partial x_i}[\mu(\frac{\partial u_i}{\partial x_j}+\frac{\partial u_j}{\partial x_j}-\frac{2}{3}\delta_{ij}\frac{\partial u_i}{\partial x_i})]+ \frac{\partial}{\partial x_i}(-\rho\overline{u_i^{'}u_j^{'}})+f_{bi} \qquad (2)$$

In the above equation u_i is i[th] Cartesian component of total velocity vector, μ is molecular viscosity, $(-\rho\overline{u_i^{'}u_j^{'}})$ is Reynolds stress, δ_{ij} is Kronecker delta and p is static pressure. The Reynolds stress should be demonstrated to near the governing equations by suitable turbulent model. For solution the RANS equation and turbulence velocity time scale, it is used by Boussinesq's eddy-viscosity supposition and two transport equations. The body force is expressed by f_{bi}.

For determination the 3D viscous incompressible flow around the ship's hull is used the ANSYS 14.0 code. The parallel version of CFX concurrently calculates the flow formulations using numerous cores of computers. The shear stress transport (SST) turbulence model had been used in this study, because it gave the best results in comparison with other turbulence models. The equations are shown as follows:

Equation of k :

$$\frac{\partial}{\partial_t}(\rho k)+\frac{\partial}{\partial x_i}(\rho k u_i)=\frac{\partial}{\partial x_j}(\Gamma_k\frac{\partial k}{\partial x_j})+G_k-Y_k+S_k \qquad (3)$$

Equation of ω:

$$\frac{\partial}{\partial_t}(\rho\omega)+\frac{\partial}{\partial x_i}(\rho\omega u_i)=\frac{\partial}{\partial x_j}(\Gamma_\omega\frac{\partial \omega}{\partial x_j})+G_\omega-Y_\omega+S_\omega \qquad (4)$$

Where G_k and G_ω express the generation of turbulence kinetic energy due to mean velocity gradients and ω . Γ_k and Γ_ω express the active diffusivity of k and ω. Y_k and Y_ω represent the dissipation of k and ω due to turbulence. D_ω expresses the cross-diffusion term, S_k and S_ω are user-defined source terms Further detail is available[14].

5.0 RESULT AND DISCUSSION

Figures 5 and 6, show the distribution of pressure coefficient on face and back surface of one blade at the radial section r/R = 0.80. It is clear that the low pressure region happens on back and the high pressure region occurred on face surface of blade.

It is clear that the low and high pressure regions occurred on back and face surfaces of blades, respectively.

Figure 5 contours of pressure coefficient on blade section

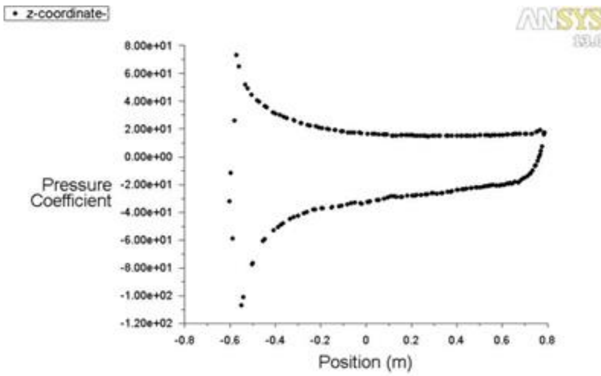

Figure 6 pressure coefficient distribution on back and face surfaces of blade section

Also, the Figure 7 shows that the distribution of low pressure and high pressure area (static pressure) on back and face surface of 5 blades, respectively. The positive pressure face of each blades make positive force to push the propeller x direction that called thrust propeller.

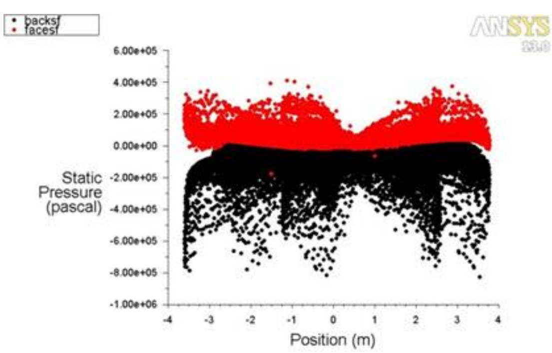

Figure 7 distribution of static pressure on face and back surfaces of 5 blades

When the propeller rotates around (x)-direction, generate thrust in (+x)-direction and high pressure occurs on face surface and low pressure on back surface of blades, respectively. [see Figures 8 and 9]. Figure 10 shows the contours of total pressure behind the propeller.

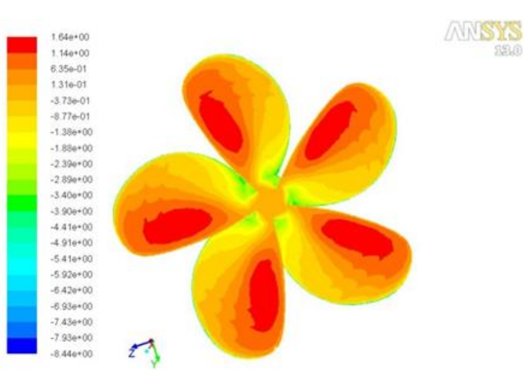

Figure 8 contours of pressure coefficient on face surface

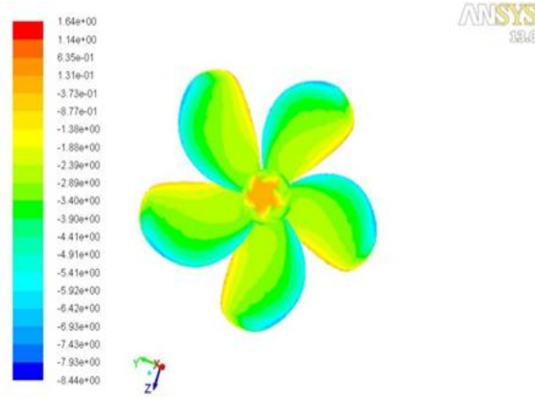

Figure 9 Contours of pressure coefficient on back surface

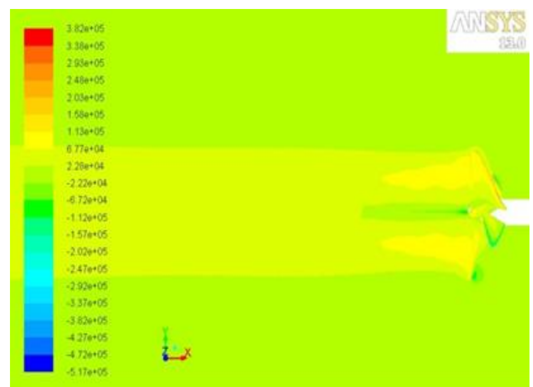

Figure 10 contours of total pressure behind the propeller

Figures 11-13, show the Contours of velocity magnitude behind the propeller, contours of velocity magnitude on face surface and velocity magnitude vectors behind the propeller, respectively. The velocity magnitude in tip of blades is higher than other region of blade surfaces. Because of the higher rotation in tips of blades, the momentum of fluid particles is very higher than near hub.

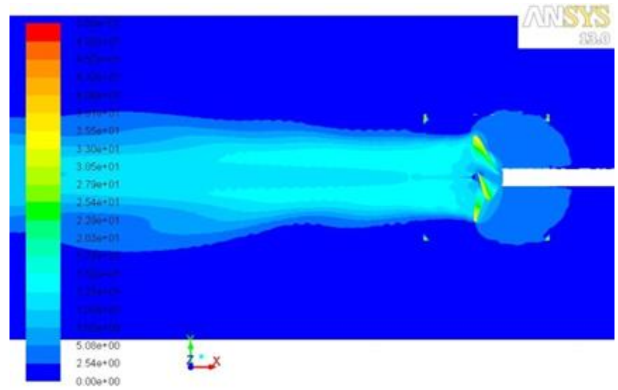

Figure 11 Contours of velocity magnitude behind the propeller

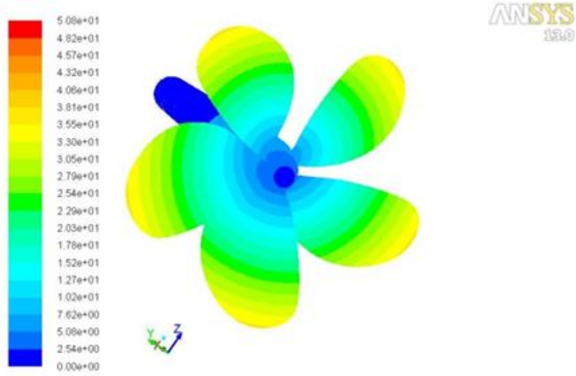

Figure 12 contours of velocity magnitude on face surface

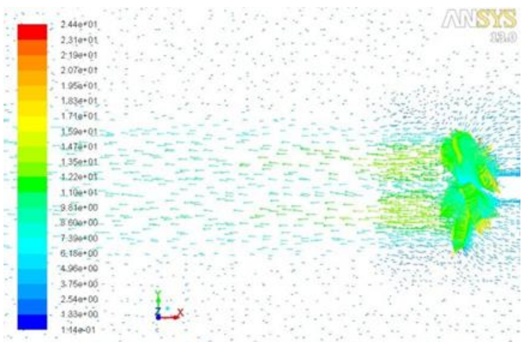

Figure 13 Velocity magnitude vectors behind the propeller

■6.0 PROPELLERPERFORMANCE

Due to the propeller model of LNG carrier has been used in experimental and numerical simulation; some similarity criteria should be applied to approach the similar results to compare the real propellers.

A series of non-dimensional specifications are used to show moments and forces that produced by propellers as followings:

Thrust coefficient: $k_t = \dfrac{T}{\rho n^2 D^4}$ (5)

Torque coefficient: $k_q = \dfrac{Q}{\rho n^2 D^5}$ (6)

Advance coefficient: $J = \dfrac{V_a}{nD}$ (7)

The results from the Numerical simulation of propeller in open water based on RANS equation of LNG ship's propeller at full scale compared to the model test results can be seen in Figure 14. Various J-values are obtained by keeping a same revolutions (n=108 rpm) but varying the flow speed. The trends of results with varying advance ratio are well predicted. It should be noted that K_Q and K_t are slightly over predicted all the way. The maximum hydrodynamic propeller efficiency will be occurred in j=0.84.

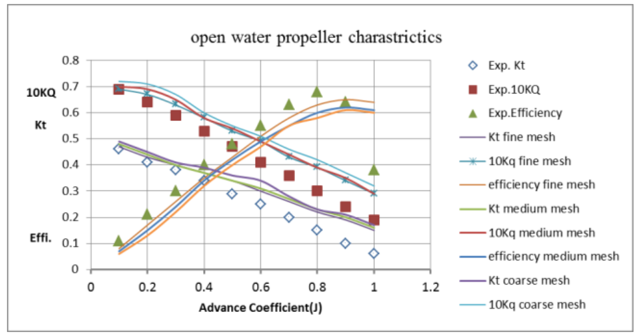

Figure 14 Propeller characteristics in open water

■7.0 CONCLUSION

Nowadays, numerical methods have been improved to estimate the flow field around the propellers and their hydrodynamics performance.

RANS (Reynolds-Averaged Navier-Stokes) methods have become a useful tool in flow analysis, engineering design and optimization. They open up new possibilities in analysis and comprehension of flow phenomena which are impossible or difficult to be implemented using traditional model tests. In accordance to the presented computational results based on RANS equations, the following conclusions are drawn:

- The propeller worked in a uniform fluid stream, producing the forces and moments, therefore, it generated the thrust and produced velocity and pressure on face blades surface and behind the propeller in the fluid flow and the fine mesh has more agreeable with experimental data in compare of medium and coarse meshes.
- The fluid velocity in the tips of face blades was higher than other areas and the fluid pressure in the face blades near leading edges was higher than other areas.
- The maximum hydrodynamic propeller efficiency occurred when j=0.84.

Acknowledgements

The authors would like to express their sincere gratitude to Universiti Teknologi Malaysia (UTM) for financial support given to this research work.

Nomenclature

D	: Propeller diameter, (m)
D_{hub}	: Hub diameter, (m)
Z	: Number of blade
P/D	: Pitch Ratio
R	: Rake of Blades
N	: Rate of revolutions of propeller, (rpm)
Cp	: Pressure coefficient
P	: Static pressure at point of interest
p_0	: Reference pressure at infinity
Va	: Advance velocity, (m/s)
J	: Advance ratio
KT	: Thrust coefficient
KQ	: Torque coefficient

Br	: Boss ratio
A_E/A_0	: Expanded Area Ratio (EAR)
ρ	: Density of water
η	: Open water efficiency
D_r	: Diameter of Rotational domain
L_r	: Length of rotational domain
$L_{mr:}$	: Outlet length of rotational domain
D_s	: Diameter of stationary domain
L_{so}	: Length of outlet stationary domain
L_{si}	: Length of inlet stationary domain
(x, y, z)	: Cartesian coordinate system with its origin at the centre of propeller
+X, +Y, +Z	: Cartesian directions in Right-Hand system
Ux,Uy,Uz	: Velocity components in the Cartesian coordinate system (x, y, z)

References

[1] Leishman, J. 1990. Dynamic Stall Experiments on the NACA 23012 Aerofoil. *Experiments in Fluids*. 9(1): 49e58.

[2] Tyler, J. C., Leishman, J. G. 1992. Analysis of Pitch and Plunge Effects on Unsteady Airfoilbehavior. *Journal of the American Helicopter Society*. 37: 69.

[3] Afrizal, E. and Koto, J. 2014. Ice Resistance Performance Analysis of Double Acting Tanker in Astern Condition. *Jurnal Teknologi (Sciences and Engineering)*. 69(7): 73–78.

[4] Junaidi, A. K., Koto, J. 2014. Parameters Study of Deep Water Subsea Pipeline Selection. 69(7): 115–119.

[5] Abyn, H., Adi Maimun, M. Rafiqul Islam, Allan Magee, Jaswar, Behnam Bodaghi, Mohamad Pauzi, C. L. Siow. 2014. Effect of Mesh Number on Accuracy of Semi Submersible Motion Prediction. Jurnal *Teknologi (Sciences & Engineering).* 66(2): 67–72.

[6] Kerwin, J. E. and C. S. Lee. 1978. Prediction of Steady and Unsteady Marine Propeller Performance by Numerical Lifting-Surface Theory. *Trans SNAME*. 86(4): 218–253.

[7] Kim, H. T. and F. Stern. 1990. Viscous Flow Around a Propeller-Shaft Configuration with Infinite-Pitch Rectangular Blades. *J. Propul*. 6: 434–443.

[8] Streckwall, H. 1986. A Method to Predict the Extent of Cavitation on Marine Propellers by Lifting-Surface-Theory. *International Symposium on Cavitation*. Sendai, Japan

[9] Abdel-Maksoud, M., F. Menter and H. Wuttke. 1998. Viscous Flow Simulations for Conventional and High-Skew Marine Propellers. *Schiffstechnik/Ship Technol. Res*. 45: 64–71.

[10] Watanabe, T., T. Kawamura, Y. Takekoshi, M. Maeda and S. H. Rhee. 2003. Simulation of Steady and Unsteady Cavitation on a Marine Propeller Using a RANS CFD Code. *5th International Symposium on Cavitation (CAV2003)*. Osaka, Japan

[11] Chen, B. and F. Stern. 1999. Computational Fluid Dynamics of Four-Quadrant Marine-Propulsor Flow. *J. Ship Res.* 43(4): 218–228.

[12] Oh, K.-J. and S. H. Kang. 1992. Numerical Calculation of the Viscous Flow Around a Rotating Marine Propeller. *KSME J.* 6(2): 140–148.

[13] Kawamura, T., Y. Takekoshi, H. Yamaguchi, T. Minowa, M.Maeda, A. Fujii, K.Kimura and T. Taketani. 2006. Simulation of unsteady Cavitating Flow Around Marine Propeller using a RANS CFD Code. In: 6th International Symposium on Cavitation (CAV2006), Wageningen, The Netherlands.

[14] Fluent 6.2 User's Manual. 2005. Ansys.